An Enhanced dq-Based Vector Control System for Modular Multilevel Converters Feeding Variable Speed Drives

Mauricio Espinoza, *Student Member*, *IEEE*, Roberto Cárdenas, *Senior Member*, *IEEE*,
Matias Diaz, *Student Member*, *IEEE*, and Jon Clare, *Senior Member*, *IEEE*

Abstract—**Modular Multilevel Converters (M²C) are considered an attractive solution for high power drive applications. However, energy balancing within the converter is complex to achieve, particularly when the machine is operating at low rotational speeds. In this paper a new control system, based on cascaded control loops and a vector-power-voltage (vPV) model of the M²C, is proposed. The control system is implemented in a dq-synchronous frame rotating at ω_e rad/s with the external loop regulating the capacitor voltages using PI controllers. The internal loop controls the converter currents using PI and resonant controllers. In addition the control systems required to operate the machine at other points, i.e. at medium and high rotational speeds, are also discussed in this work. Experimental results obtained with a M²C-based drive laboratory prototype with eighteen power cells are presented in this paper.**

Index Terms—**Modular Multilevel Converter, variable speed drives, low-frequency operation, voltage balancing.**

Fig. 1. Modular Multilevel Converter topology

I. INTRODUCTION

THE Modular Multilevel Converter (M²C) is a relatively new power converter topology originally proposed for high voltage dc (HVDC) transmission [1]–[4]. However, for drive applications, the M²C has several advantages when compared to other high-power converters, particularly for quadratic torque-speed profile loads, where a better performance has been reported [5], [6]. Several publications, where experimental results are presented, have been discussed in the literature [7]–[20]. The topology of a high power drive based on a M²C is shown in Fig. 1. It is composed of an ac port, a dc port and six "clusters". Each cluster has n cascaded cells and an inductor L. Each cell is composed of a half bridge circuit and its associated "flying" capacitor C.

Because of the large number of flying capacitors, one of the important tasks of the control systems is to maintain the voltage in each capacitor operating within an acceptable range.

Mauricio Espinoza is with the Electrical Engineering Department, University of Costa Rica, San Pedro, Costa Rica (e-mail: mauricio.espinoza_bola@ucr.ac.cr),

Roberto Cárdenas and Matías Díaz are with the Electrical Engineering Department, University of Chile, Avenida Tupper 2007, Santiago, Chile (e-mail: rcd@ieee.org, mdiaz@ing.uchile.cl).

Jon Clare is with the Department of Electrical and Electronic Engineering, University of Nottingham, Nottingham University Park, Nottingham, NG7, 2RD, (e-mail: jon.clare@nottingham.ac.uk).
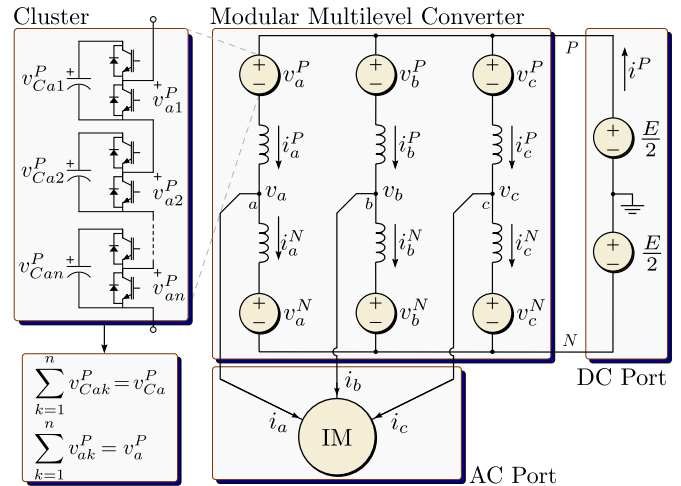
This control target is difficult to fulfil when the electrical machine is operating at zero or low rotational speed [12], [13]. Therefore, for control purposes, the operating range of the M²C is usually divided into two modes: The High-Frequency Mode (HFM) and the Low-Frequency Mode (LFM).

Control systems for both, HFM and LFM, have been presented and experimentally validated in [9]–[12]. However, in these papers the control systems are not decoupled. Therefore, cross-couplings between control loops is possible, affecting the overall system performance. Moreover, in [9]–[12], [19] the regulation of the currents and voltages is realized using P or PI controllers. As is well known, these controllers are not appropriate for regulating the ac currents and voltages found in the M²C with zero steady state error [21]. In [19] a decoupled model of the M²C is proposed using a six-dimensional transformation of the converter signals to regulate the variables at each port and to perform the energy balance of the M²C. However, the effectiveness of the algorithms proposed in [19] is difficult to evaluate because the presented experimental results do not show the tracking achieved for these signals in the proposed six-dimensional domain.

To balance the converter energy in the LFM, the use of circulating currents and common mode voltages has been proposed and analysed in several publications [12]–[16], [22]. The waveforms proposed in the literature for the common mode voltage and mitigation currents are sinusoidal signals

with or without third harmonic injection [12], [13], square wave [12] and hybrid mitigation signals [16], [22]. In all these publications, the set points for the regulation of the mitigation currents are predefined off-line. Therefore, the predetermined mitigation currents do not have any sort of closed loop adaptation capability which is required to compensate for possible changes in the parameters or operating points of the M²C-based drive. For instance off-line predefined mitigation signals cannot compensate non-linearities (e.g. dead times issues in the converter cells); non-idealities or simplifications in the power converter model (e.g. neglected inductor voltage in the energy model); the difficulties associated with measuring the stator voltage at low rotational speeds, etc. Moreover in [12]–[16], [19], [22] P or PI controllers, implemented in the stationary frame, are utilised. As mentioned before, these controllers are not appropriate to regulate sinusoidal signals with zero steady state error.

To solve the aforementioned problems, this paper proposes a new control system for the operation of the M²C-based drive. Moreover, to analyse the control system a vector-Power-Voltage (vPV) model is presented in this work. This model represents the dynamics of the topology shown in Fig. 1 using a compact notation with only four vector equations being required. Moreover, it is simpler to use this 4-equation modelling to propose, analyse, and implement conventional dq-based vector control systems.

The proposed dq vector control system is based on a cascaded architecture, where the outer loop drives the imbalances in the capacitor voltages to zero by modifying the set-point value for the circulating currents, which are regulated with resonant controllers implemented in a synchronous rotating frame. Using some minor modifications the proposed control scheme is suitable for operation in both the LFM and HFM.

The rest of this paper is organised as follows. Section II briefly discusses the conventional modelling of the M²C drive topology shown in Fig. 1. Section III discussed the proposed vPV model and the vector control systems for operating at LFM and HFM. Section IV presents the experimental results obtained with a laboratory prototype. Finally, an appraisal of the proposed control systems is presented in the conclusions.

II. ANALYSIS OF THE M²C

A. Voltage-Current Model of the M²C

As often occurs in applications related to power converters, it is simpler to analyse the system using a different coordinate space. In this section the $\Sigma\Delta\alpha\beta 0$ transformation (which is partly based on the work presented in [23]) is discussed. Considering the M²C shown in Fig. 1, the following currents can be obtained as a function of the cluster currents by using the $[C]_{\Sigma\Delta}$ matrix, which considers the interaction of electrical variables among the converter poles:

$$\begin{bmatrix} i_a^\Sigma & i_b^\Sigma & i_c^\Sigma \\ i_a & i_b & i_c \end{bmatrix} = \underbrace{\begin{bmatrix} \frac{1}{2} & \frac{1}{2} \\ 1 & -1 \end{bmatrix}}_{[C]_{\Sigma\Delta}} \cdot \begin{bmatrix} i_a^P & i_b^P & i_c^P \\ i_a^N & i_b^N & i_c^N \end{bmatrix} \tag{1}$$

where the lower row of the resultant current matrix contains the ac port currents and the upper row contains currents that

do not appear at the ac port, usually referred to as circulating currents [12], [24]. However, (1) can be post-multiplied by the transpose Clarke-transformation, $[C]_{\alpha\beta 0}^\mathsf{T}$, to consider the interaction of the electrical variables among the converter phases of the M²C and to get the independent components of each kind of current, resulting in:

$$\begin{bmatrix} i_\alpha^\Sigma & i_\beta^\Sigma & i_0^\Sigma \\ i_\alpha & i_\beta & i_0 \end{bmatrix} = \begin{bmatrix} \frac{1}{2} & \frac{1}{2} \\ 1 & -1 \end{bmatrix} \cdot \begin{bmatrix} i_a^P & i_b^P & i_c^P \\ i_a^N & i_b^N & i_c^N \end{bmatrix} \cdot \underbrace{\begin{bmatrix} \frac{2}{3} & -\frac{1}{3} & -\frac{1}{3} \\ 0 & \frac{1}{\sqrt{3}} & -\frac{1}{\sqrt{3}} \\ \frac{1}{3} & \frac{1}{3} & \frac{1}{3} \end{bmatrix}^\mathsf{T}}_{[C]_{\alpha\beta 0}^\mathsf{T}}$$

$$= \begin{bmatrix} i_\alpha^\Sigma & i_\beta^\Sigma & \frac{1}{3}i^P \\ i_\alpha & i_\beta & 0 \end{bmatrix} \tag{2}$$

where $i_0^\Sigma = \frac{1}{3}i^P$ and the zero sequence current is $i_0 = 0$.

The $\Sigma\Delta\alpha\beta 0$ transformation applied to (2) could be used to transform any 2×3 matrix from *PNabc* coordinates to $\Sigma\Delta\alpha\beta 0$ coordinates. Mathematically this is written as:

$$[X]_{\alpha\beta 0}^{\Sigma\Delta} \doteq [C]_{\Sigma\Delta} \cdot [X]_{abc}^{PN} \cdot [C]_{\alpha\beta 0}^\mathsf{T} \tag{3}$$

Hence, Kirchhoff's voltage law for every loop of Fig. 1 is applied to obtain the dynamic model of the cluster currents:

$$\frac{E}{2} \begin{bmatrix} 1 & 1 & 1 \\ 1 & 1 & 1 \end{bmatrix} = \begin{bmatrix} v_a^P & v_b^P & v_c^P \\ v_a^N & v_b^N & v_c^N \end{bmatrix} + L\frac{d}{dt}\begin{bmatrix} i_a^P & i_b^P & i_c^P \\ i_a^N & i_b^N & i_c^N \end{bmatrix}$$

$$+ \begin{bmatrix} v_a & v_b & v_c \\ -v_a & -v_b & -v_c \end{bmatrix} \tag{4}$$

and applying the $\Sigma\Delta\alpha\beta 0$ transformation to (4) yields:

$$\begin{bmatrix} 0 & 0 & \frac{1}{2}E \\ 0 & 0 & 0 \end{bmatrix} = \begin{bmatrix} v_\alpha^\Sigma & v_\beta^\Sigma & v_0^\Sigma \\ v_\alpha^\Delta & v_\beta^\Delta & v_0^\Delta \end{bmatrix} + L\frac{d}{dt}\begin{bmatrix} i_\alpha^\Sigma & i_\beta^\Sigma & \frac{1}{3}i^P \\ i_\alpha & i_\beta & 0 \end{bmatrix}$$

$$+ 2\begin{bmatrix} 0 & 0 & 0 \\ v_\alpha & v_\beta & v_0 \end{bmatrix} \tag{5}$$

where v_α, v_β, i_α and i_β are the $\alpha\beta$ coordinates of the voltages and currents in the electrical machine, v_0 is the common mode voltage and i_α^Σ and i_β^Σ are circulating currents which are not present at any port. Using (5) it is simpler to propose and analyse an appropriate control system to regulate each independent current of the M²C shown in Fig. 1.

B. Power-Voltage Model of the M²C

The sum of the capacitor voltages in a cluster (i.e. the available cluster voltage) is related with its instantaneous power by the following expression [10], [25]:

$$\frac{d}{dt}\underbrace{\begin{bmatrix} v_{Ca}^P & v_{Cb}^P & v_{Cc}^P \\ v_{Ca}^N & v_{Cb}^N & v_{Cc}^N \end{bmatrix}}_{[V]_{Cabc}^{PN}} \approx \frac{1}{Cv_C^*}\underbrace{\begin{bmatrix} p_a^P & p_b^P & p_c^P \\ p_a^N & p_b^N & p_c^N \end{bmatrix}}_{[P]_{abc}^{PN}} \tag{6}$$

where v_C^* is the voltage reference for the capacitor voltage in each cell. Notice that the powers in (6) (in a-b-c coordinates) are calculated using the current and voltage of each cluster (e.g. $p_a^P = v_a^P i_a^P$, $p_a^N = v_a^N i_a^N$, etc.). Moreover, in (6) it is assumed that the capacitor voltages are well regulated with instantaneous values close to v_C^*.

The $\Sigma\Delta\alpha\beta 0$ transformation can be applied to (6) to relate the total cluster voltage and the power flow in each cluster

among the converter poles and phases [see (3)] as follows:

$$\frac{d}{dt}\underbrace{\begin{bmatrix} v_{C\alpha}^{\Sigma} & v_{C\beta}^{\Sigma} & v_{C0}^{\Sigma} \\ v_{C\alpha}^{\Delta} & v_{C\beta}^{\Delta} & v_{C0}^{\Delta} \end{bmatrix}}_{[V]_{C\alpha\beta 0}^{\Sigma\Delta}} \approx \frac{1}{Cv_C^*}\underbrace{\begin{bmatrix} p_{\alpha}^{\Sigma} & p_{\beta}^{\Sigma} & p_0^{\Sigma} \\ p_{\alpha}^{\Delta} & p_{\beta}^{\Delta} & p_0^{\Delta} \end{bmatrix}}_{[P]_{\alpha\beta 0}^{\Sigma\Delta}} \qquad (7)$$

where the powers in $\Sigma\Delta\alpha\beta 0$ coordinates could be derived from (5). After some manipulations yields:

$$p_{\alpha}^{\Sigma} = \tfrac{1}{2}Ei_{\alpha}^{\Sigma} - \tfrac{1}{4}i_{\alpha}v_{\alpha} + \tfrac{1}{4}i_{\beta}v_{\beta} - \tfrac{1}{2}i_{\alpha}v_0 \qquad (8a)$$

$$p_{\beta}^{\Sigma} = \tfrac{1}{2}Ei_{\beta}^{\Sigma} + \tfrac{1}{4}i_{\beta}v_{\alpha} + \tfrac{1}{4}i_{\alpha}v_{\beta} - \tfrac{1}{2}i_{\beta}v_0 \qquad (8b)$$

$$p_0^{\Sigma} = \tfrac{1}{6}Ei^{P} - \tfrac{1}{4}i_{\alpha}v_{\alpha} - \tfrac{1}{4}i_{\beta}v_{\beta} \qquad (8c)$$

$$p_{\alpha}^{\Delta} = \tfrac{1}{2}Ei_{\alpha} - \tfrac{2}{3}i^{P}v_{\alpha} - i_{\alpha}^{\Sigma}v_{\alpha} + i_{\beta}^{\Sigma}v_{\beta} - 2i_{\alpha}^{\Sigma}v_0 \qquad (8d)$$

$$p_{\beta}^{\Delta} = \tfrac{1}{2}Ei_{\beta} - \tfrac{1}{3}2i^{P}v_{\beta} + i_{\beta}^{\Sigma}v_{\alpha} + i_{\alpha}^{\Sigma}v_{\beta} - 2i_{\beta}^{\Sigma}v_0 \qquad (8e)$$

$$p_0^{\Delta} = -i_{\alpha}^{\Sigma}v_{\alpha} - i_{\beta}^{\Sigma}v_{\beta} - \tfrac{2}{3}i^{P}v_0 \qquad (8f)$$

The meaning of these variables is discussed in next sections.

III. PROPOSED CONTROL SYSTEM

A. Vector Power-Voltage Model of the M²C

In this paper a new Vector-Power-Voltage (vPV) model of the M²C is proposed. This model allows a simple analysis and implementation of control strategies using vector control algorithms. Defining the power flows and the total cluster voltages as vectors, e.g. $\underline{p}_{\alpha\beta}^{\Sigma} = p_{\alpha}^{\Sigma} + jp_{\beta}^{\Sigma}$, $\underline{v}_{C\alpha\beta} = v_{C\alpha} + jv_{C\beta}$, etc., and using the conventional vector notation for the currents and voltages, the vector model of (8a)-(8f) is obtained as:

$$\underline{p}_{\alpha\beta}^{\Sigma} = \tfrac{1}{2}E\underline{i}_{\alpha\beta}^{\Sigma} - \tfrac{1}{4}\left(\underline{i}_{\alpha\beta}\underline{v}_{\alpha\beta}\right)^{c} - \tfrac{1}{2}v_0\underline{i}_{\alpha\beta} \qquad (9a)$$

$$\underline{p}_{\alpha\beta}^{\Delta} = \tfrac{1}{2}E\underline{i}_{\alpha\beta} - \tfrac{2}{3}i^{P}\underline{v}_{\alpha\beta} - \left(\underline{v}_{\alpha\beta}\underline{i}_{\alpha\beta}^{\Sigma}\right)^{c} - 2v_0\underline{i}_{\alpha\beta}^{\Sigma} \qquad (9b)$$

$$p_0^{\Sigma} = \tfrac{1}{6}Ei^{P} - \tfrac{1}{4}\left(\underline{v}_{\alpha\beta} \circ \underline{i}_{\alpha\beta}\right) \qquad (9c)$$

$$p_0^{\Delta} = -\left(\underline{v}_{\alpha\beta} \circ \underline{i}_{\alpha\beta}^{\Sigma}\right) - \tfrac{2}{3}i^{P}v_0 \qquad (9d)$$

where the symbol "$\circ$" represents the dot product between vectors and the superscript "c" stands for the complex conjugated operator. In (9a), the vector $\underline{p}_{\alpha\beta}^{\Sigma}$ represents the power flows between the converter phases. On the other hand the vector power $\underline{p}_{\alpha\beta}^{\Delta}$ [see (9b)] and the zero sequence power p_0^{Δ} [see (9d)] represents power flows between the upper and lower poles of the converter. Finally the zero sequence power, p_0^{Σ} [see (9c)] is proportional to the power flow between the dc and ac ports and defines the change in the M²C total stored energy. The relationship between the powers of (9) and the voltages in $\Sigma\Delta\alpha\beta 0$ coordinates is obtained from (7).

If the control systems of the M²C-based drive depicted in Fig. 1 achieve perfect regulation of the capacitor voltages, then it is concluded from (6) and (7) that in steady state the vector voltages in $\Sigma\Delta\alpha\beta 0$ coordinates converge to:

$$\left|\underline{v}_{C\alpha\beta}^{\Sigma*}\right| = \left|\underline{v}_{C\alpha\beta}^{\Delta*}\right| = v_{C0}^{\Delta*} = 0, \qquad v_{C0}^{\Sigma*} = nv_C^* \qquad (10)$$

B. Analysis of the System Using the vPV Model for LFM

When the machine is operating at $\omega_e \approx 0\ rads^{-1}$, the stator voltage applied is low. Using (7) and (9b) yields:

$$Cv_C^*\frac{dv_{C\alpha\beta}^{\Delta}}{dt} \approx \underline{p}_{\alpha\beta}^{\Delta} \approx \tfrac{1}{2}E\underline{i}_{\alpha\beta} - 2v_0\underline{i}_{\alpha\beta}^{\Sigma} \qquad (11)$$

Analysing (11) is concluded that most of the low frequency ω_e power oscillations are produced by the term $E\underline{i}_{\alpha\beta}$, particularly when high motor starting current is required. Moreover, if the stator voltage is not negligible, additional low frequency power oscillations are produced by the term $i^{P}\underline{v}_{\alpha\beta}$ in $\underline{p}_{\alpha\beta}^{\Delta}$.

To avoid large voltage variations in the M²C capacitors, the low frequency power oscillations produced by $E\underline{i}_{\alpha\beta}$ and $i^{P}\underline{v}_{\alpha\beta}$ have to be mitigated or eliminated from $\underline{p}_{\alpha\beta}^{\Delta}$. Therefore, in this work a hybrid control strategy, based on the ac component of the common mode voltage (i.e. $\tilde{v}_0$) and the circulating current (i.e. $\tilde{\underline{i}}_{\alpha\beta}^{\Sigma}$), is proposed to reduce the amplitude of $\underline{v}_{C\alpha\beta}^{\Delta}$ during LFM operation. Thus, the set point value of the circulating current $\tilde{\underline{i}}_{\alpha\beta}^{\Sigma}$ is defined as:

$$\tilde{\underline{i}}_{\alpha\beta}^{\Sigma*} = ke^{j(\theta_e - \theta_0)}f(t) \qquad (12)$$

where k is a constant, $\theta_e = \int \omega_e dt$, with ω_e as the output frequency and θ_0 a phase angle. The term $f(t)$ is defined as:

$$f(t) = A\sin(\omega_m t) \qquad (13)$$

where the value of ω_m is a degree of freedom, usually selected to be relatively high compared to ω_e. Additionally, $\tilde{v}_0^*$ is defined as a square waveform of frequency ω_m, i.e.:

$$\tilde{v}_0^* = V_0 \text{sgn}\left[f(t)\right] \qquad (14)$$

Using (12) and (14) is relatively simple to demonstrate that $\tilde{v}_0^*\tilde{\underline{i}}_{\alpha\beta}^{\Sigma*}$ has a power term of frequency ω_e which could be used to mitigate the low frequency power pulsations produced by the terms $E\underline{i}_{\alpha\beta}$ and $\underline{v}_{\alpha\beta}$ in (9b). Ideally, these low frequency signals are completely eliminated when:

$$\tilde{\underline{i}}_{\alpha\beta}^{\Sigma} = ke^{j(\theta_e - \theta_0)}f(t) = \tfrac{1}{2V_0}\left(\tfrac{1}{2}E\underline{i}_{\alpha\beta} - \tfrac{2}{3}i^{P}\underline{v}_{\alpha\beta}\right)f(t) \qquad (15)$$

where A=1.57 is used in (13) as is discussed elsewhere [22].

In the following subsections the control systems required for voltage balancing and mitigation of the power oscillations are going to be discussed. They are analysed and designed using the vPV model depicted in (9a)-(9d).

C. Vector control of the $\underline{v}_{C\alpha\beta}^{\Delta}$ voltage

1) At low rotational speed (LFM): As discussed in several publications [12]–[16], [22] the most critical operating point of a M²C-drive is when the electrical frequency is low and the machine is operating with a relatively high current. Moreover, if $\tilde{\underline{i}}_{\alpha\beta}^{\Sigma*}$ is off-line calculated using (15), there are several issues which can potentially hinder the correct mitigation of the low frequency voltage pulsation in the M²C capacitors. Some of these issues have been discussed at Section I. Therefore, in this operating conditions a control systems with good dynamic response and zero steady state error is fundamental to achieve a proper regulation of the capacitor voltages. To fulfil these requirements, in this paper a closed loop vector control system
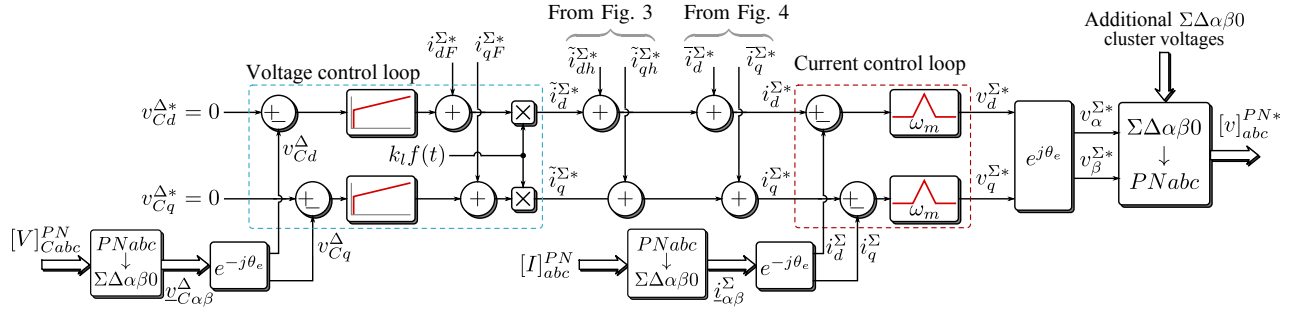
Fig. 2. Proposed control system for the voltage vector $\underline{v}^{\Delta}_{C\alpha\beta}$ at LFM

for real time regulation of $\tilde{\underline{i}}^{\Sigma*}_{\alpha\beta}$ is proposed. The performance of this control system is good considering the high dynamic typically achievable with vector control techniques.

To analyse the proposed nested control loops in dq-coordinates, the dynamics of the system is referred to a synchronous frame. Therefore, replacing (7) in (9b) and referring to a dq-axis rotating at ω_e yields:

$$Cv^*_C\left[\frac{dv^{\Delta}_{Cdq}}{dt} + j\omega_e\underline{v}^{\Delta}_{Cdq}\right] \approx \frac{1}{2}Ei_{dq} - \frac{2}{3}i^P\underline{v}_{dq} - 2v_0i^{\Sigma}_{dq} \qquad (16)$$

Notice that in (16) one term producing relatively high frequency power oscillations has not been considered. These oscillations are almost completely filtered out by the M²C capacitors and its effects are negligible.

The proposed nested control system is shown in Fig. 2. The slower outer control loop regulates $\underline{v}^{\Delta}_{Cdq}$, and the internal faster control loop regulates the circulating current $\tilde{\underline{i}}^{\Sigma*}_{dq}$. The voltage vector $\underline{v}^{\Delta}_{Cdq}$, is controlled, with zero steady state error, using PI controllers. The output of the external control loop is used to calculate the set-point for the circulating currents $\tilde{\underline{i}}^{\Sigma}_{dq}$. For simplicity, the dq decoupling terms have not been considered in Fig. 2, but they can be added to both control loops.

In the external loop at the output of the PI controllers, two feed-forward compensation terms are considered. These terms are obtained by transforming (15) to the dq frame yielding:

$$\tilde{\underline{i}}^{\Sigma*}_{dqF} = \frac{1}{2V_0}\left(\frac{1}{2}Ei_{dq} - \frac{2}{3}i^P\underline{v}_{dq}\right)f(t) \qquad (17)$$

and they correspond to the conventional feed-forward terms used in the control strategies reported in [12]. In this work these terms are used only to improve the dynamic performance of the voltage control loop. However, if (for instance) some of the components in (17) are misidentified, the PI controllers still ensure zero steady state error driving $\underline{v}^{\Delta}_{Cdq}$ to zero (i.e. eliminating the ω_e frequency component in $\underline{v}^{\Delta}_{C\alpha\beta}$).

Analysing (13) and (17) is concluded that the dq circulating currents have sinusoidal components of frequency ω_m. Therefore, in this work resonant controllers are utilised to regulated these currents (see Fig. 2). Notice that the magnitude and phase of $\tilde{\underline{i}}^{\Sigma*}_{\alpha\beta}$ (i.e. k and θ_0) are modified by the voltage control loop. This is certainly an advantage over the conventional mitigation algorithm, where $\tilde{\underline{i}}^{\Sigma*}_{\alpha\beta}$ is predetermined in advance and P or PI controllers, implemented in the stationary frame, are used in the control system to balance the capacitor voltages [12], [19].

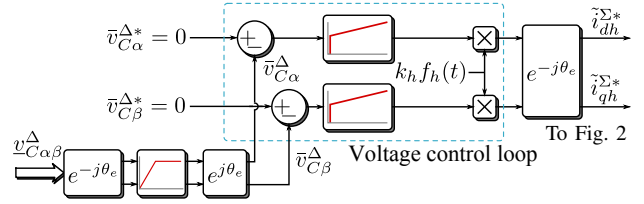The output of the cascaded control systems shown in Fig.

Fig. 3. Proposed control system for the voltage $\underline{v}^{\Delta}_{C\alpha\beta}$ at HFM

2 are the clusters voltages in $\Sigma\Delta\alpha\beta0$ coordinates. These voltages are referred to the $PNabc$ frame using the inverse $\Sigma\Delta\alpha\beta0$ transformation in order to be processed by the cell balancing algorithm (see [26]). In this work the angle θ_e is the rotor-flux angle of the vector controlled induction machine. However, the control system proposed in Fig. 2 can be orientated along any other vector rotating at ω_e $rads^{-1}$.

2) Operation at high rotational speed (HFM): The M²C is operating in the HFM when the voltage oscillations in $\underline{v}^{\Delta}_{C\alpha\beta}$ are relatively small and the circulation of the mitigation currents is not longer required to maintain this voltage bounded.

In the HFM only the dc components of $\underline{v}^{\Delta}_{C\alpha\beta}$ are regulated to zero. Hence, PI controllers implemented in the stationary frame are used, as is shown in the control system in Fig. 3. To eliminate the components of frequency ω_e from $\underline{v}^{\Delta}_{Cdq}$, a filter is applied. Good performance and implementation simplicity have been obtained by using a high-pass filter implemented in a synchronous frame rotating at ω_e (see Fig. 3). Notice that high pass filters implemented in a dq-frame are equivalent to notch filters in the stationary frame.

In previous work [19] it was proposed to add a positive and negative sequence current of frequency ω_e to $\underline{i}^{\Sigma}_{\alpha\beta}$, to produce a manipulable power flow in $(\underline{v}_{\alpha\beta}\underline{i}^{\Sigma}_{\alpha\beta})^c$ and $(\underline{v}_{\alpha\beta}\circ\underline{i}^{\Sigma}_{\alpha\beta})$. These power flows were used to control the voltages $\underline{v}^{\Delta}_{C\alpha\beta}$ and v^{Δ}_{C0} [see (9b) and (9d)]. However, when that methodology is used, the M²C control system could be affected by sudden variations of the machine stator voltage, $\underline{v}_{\alpha\beta}$. In fact, cross-couplings between the control systems could be introduced when $\underline{v}_{\alpha\beta}$ is affected by intermittent load perturbations.

Hence, in this paper the power term $v_0i^{\Sigma}_{\alpha\beta}$ in (9b) is used to balance the voltage vector $\underline{v}^{\Delta}_{C\alpha\beta}$ at HFM operation. Moreover, the common mode voltage $\tilde{v}_0$ is used to increase the maximum modulation index of the M²C using third harmonic injection. Then, for the operation in the high frequency mode the voltage
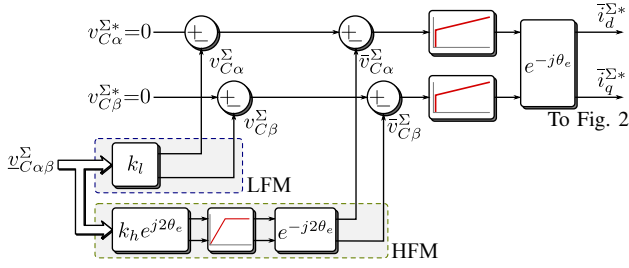
Fig. 4. Control system to regulate the voltage $\underline{v}^\Sigma_{\alpha\beta}$

Fig. 5. Proposed control system for the voltages v^Σ_{C0} and v^Δ_{C0}

$\tilde{v}_0$ and the function $f_h(t)$ are defined as:

$$\tilde{v}_0 = V_{0h} \sin\left(3\theta^\Delta_{\alpha\beta}\right), \qquad f_h(t) = 2\sin\left(3\theta^\Delta_{\alpha\beta}\right) \qquad (18)$$

where $\theta^\Delta_{\alpha\beta}$ is defined as the electrical angle of the vector $\underline{v}^\Delta_{\alpha\beta} = v^\Delta_\alpha + jv^\Delta_\beta$. It is important to clarify that the electrical angle used to generate the common mode voltage ($3\theta^\Delta_{\alpha\beta}$) is not directly derived from the voltages applied to the machine stator. This is because the phase shift introduced by the voltage drop in the cluster inductances is not negligible.

3) Transition between modes: A simple method is used to switch between the low frequency and high frequency operating modes. Assuming that ω_l is the highest frequency at which (only) the LFM is used and the transition zone is from ω_l to ω_h, the following weighting factors are defined:

$$k_l = 1 - k_h = \begin{cases} 1 & \text{if } |\omega_e| < \omega_l \\ \frac{\omega_h - |\omega_e|}{\omega_h - \omega_l} & \text{if } \omega_l \le |\omega_e| \le \omega_h \\ 0 & \text{if } \omega_h < |\omega_e| \end{cases} \qquad (19)$$

These weighting factors are used to select the reference for current $\underline{i}^{\Sigma*}_{dq}$ for either HFM or LFM (see Fig. 2 and Fig. 3). For the experimental work presented in Section IV, the value of ω_l is $20\pi\ rads^{-1}$ ($\omega_r \approx 500$rpm) and ω_h is equal to 30π $rads^{-1}$ ($\omega_r \approx 750$rpm).

D. Control of $\underline{v}^\Sigma_{\alpha\beta}$ for the whole speed operating range

The voltage $\underline{v}^\Sigma_{C\alpha\beta}$ is regulated by manipulating $\underline{p}^\Sigma_{\alpha\beta}$ of (9a). However, in $\underline{p}^\Sigma_{\alpha\beta}$ there are not large low frequency power oscillation when the machine is operating at $\omega_e \approx 0$ and a single control loop (see Fig. 4) with some minor modifications could suffice to operate in the LFM as well as the HFM.

The regulation of $\underline{v}^\Sigma_{C\alpha\beta}$ is achieved by introducing a dc component in the circulating currents, $\overline{\underline{i}}^{\Sigma*}_{\alpha\beta}$, which affects the power $E\underline{i}^\Sigma_{\alpha\beta}$ in (9a). The proposed control system is shown in Fig. 4. At LFM, the voltage $\underline{v}^\Sigma_{C\alpha\beta}$ is directly used as a feedback signal, because most of its ac components are in the high frequency range which are filtered out by the cell capacitors. The only exception is the term $(\underline{v}_{\alpha\beta}\underline{i}_{\alpha\beta})^c$ that produce a power component of frequency $2\omega_e$. However, for LFM operation, the magnitude of the stator voltage $\underline{v}_{\alpha\beta}$ is small and the effects produced by this power term are typically negligible.

To avoid the oscillations introduced by the $2\omega_e$ frequency component at HFM operation, a notch filter (implemented synchronously) is applied to the feedback signal. The transition between modes is also realised using the weighting factors k_l
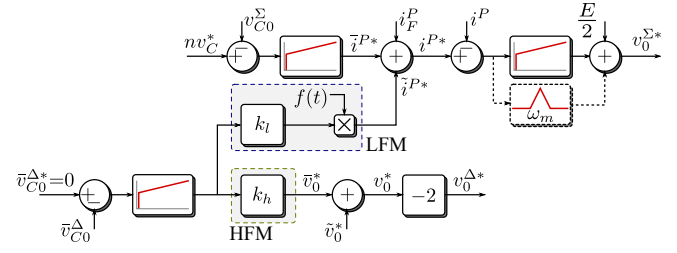
and k_h. The output of the PI controllers is a dc component added to the circulating current reference $\underline{i}^{\Sigma*}_{\alpha\beta}$ (see Fig. 2).

E. Control of the voltages v^Σ_{C0} and v^Δ_{C0}

The voltages v^Σ_{C0} and v^Δ_{C0} are controlled by manipulating the current i^P and the common mode voltage, $\overline{v}_0$. The proposed control system, for both voltages, is shown in Fig. 5.

The voltage v^Σ_{C0} is controlled by regulating the power produced by the term Ei^P using the current i^P [see (9c)] as shown in the top side of Fig. 5. A feed-forward i^P_F term could be included to improve the dynamic response when sudden variations in the ac output power are produced. This output power is represented by the term $\frac{1}{4}(\underline{v}_{\alpha\beta} \circ \underline{i}_{\alpha\beta})$ in (9c).

The voltage v^Δ_{C0} is regulated by manipulating the power produced by the term $i^P v_0$ in (9d). This is achieved by introducing a dc component in the common mode voltage v_0 as shown at the bottom of Fig. 5. However, when the machine is operating at low rotational speed, the input power is negligible and the current i^P is very low. Therefore in this case the regulation of v^Δ_{C0} could require a large dc component in the common mode voltage v_0. To avoid this problem, in this paper an alternative control method for LFM operation is proposed.

It is relatively simple, with a low control effort, to add an ac ($\tilde{i}^P$) current superimposed to the main dc input current. If the current $\tilde{i}^P$ has the same frequency and phase of $f(t)$ [see (13)], then the voltage v^Δ_{C0} could be regulated by manipulating the amplitude of ($\tilde{i}^P$) and the mean value of the power term $\tilde{i}^P v_0$ in (9d). The proposed control system is shown in Fig. 5. Notice that a resonant controller tuned at ω_m could be required to regulate $\tilde{i}^P$. Moreover the use of an ac component superimposed to the main dc input current is dependant on the capacity of the dc power supply (feeding the M²C) to withstand operation with ac current components.

The selection of the control systems for HFM/LFM operation is again realised by using the weighting factors of (19).

IV. EXPERIMENTAL SET-UP AND RESULTS

In Fig. 6a the experimental system implemented to validate the proposed control strategy is shown. In addition a picture of the experimental prototype is shown in Fig. 6b.

The M²C prototype is fed by a dc-link created by a six-pulse diode rectifier bridge and filter capacitors. The M²C output port is connected to a 3kW, 2910rpm, 2-pole vector-controlled induction machine driving a Permanent Magnet Generator (PMG). The PMG is feeding a 3ϕ resistor bank
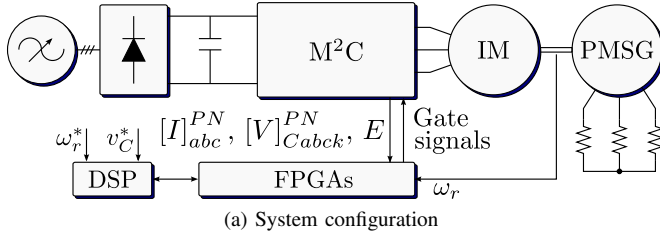
(a) System configuration
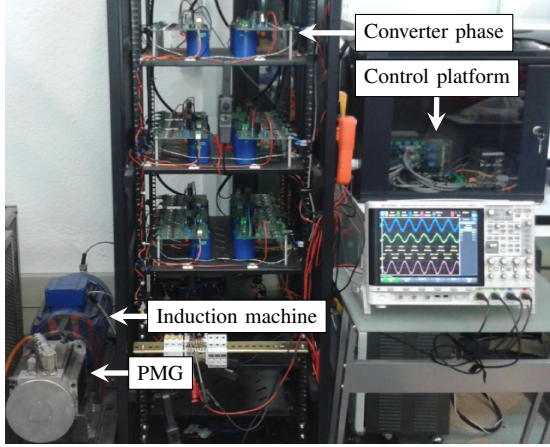
(b) Experimental system

Fig. 6. Description of the laboratory prototype

TABLE I
SET-UP PARAMETERS FOR THE 18 CELLS M^{2}C-DRIVE

Parameter	Symbol	Value	Unit
dc port voltage	E	450	V
Cluster inductor	L_1	2,5	mH
Cell capacitor	C	4700	μF
Cell dc voltage	V_C	160	V
Switching frequency	f_s	5000	Hz
Mitigating frequency	ω_m	314	rad/s

emulating a quadratic torque-speed load. For the implementation of the indirect vector-control system [27], a position encoder of 10.000 pulses per revolution is affixed to the induction machine. Hall effect transducers are used to measure the dc-link voltage, the capacitor voltage of the 18 cells and the cluster currents. To control the system a platform based on two FPGA boards (Actel ProASIC3), 40 14-bit AD channels and the DSP Texas Instrument TMS320C6713 is used. Optical fibres are used to transmit the switching signals. The experimental parameters are summarized in Table I. All the control systems have been tuned using frequency domain linear control tools. The controllers are designed with the same tuning parameters to allow a fair comparison between different control methodologies.

A. Experimental results considering operation at $\omega_r = 0$

For this test the rotor of the induction machine is mechanically locked and the stator currents are regulated to $i_d \approx 2.2$A and $i_q = 10$A. This is a very demanding condition for the M^{2}C control system considering that the electrical frequency (close

to 1.6Hz) is equal to the slip frequency. Two control system have been implemented to obtain the experimental results shown in Fig. 7. In both cases, the function $f(t)$ was defined as in (13) and the common mode voltage waveform was changed to a trapezoidal shape, with the edges of the 50Hz trapezoidal wave varying between -100% to 100% of the peak value in approximately 1ms. With this modification, the performance of the proposed control systems to operate when variations are produced in the M^{2}C system is validated.

To allow a fair comparison between different control methodologies, all the nested control loops discussed in this work have been designed using identical tuning algorithms. Firstly, for the inner control loops (see Fig. 2), the controller parameters have been calculated by solving the following constrained optimisation problem:

$$\min_{\underline{\lambda}} \sum_{h=0}^{\infty} |e(hT_s)| \text{ such that: } M_S = 2 \qquad (20)$$

where $\underline{\lambda}$ is the vector that contains the controller parameters, e is the tracking error, T_s the sampling time and M_s is the sensitivity function [28]. Notice that a system with $M_S \leq 2$ is usually considered very robust [28], [29].

Secondly, the parameters of the outer controllers are calculated by solving the following constrained optimisation problem:

$$\min_{\underline{\lambda}} \sum_{h=0}^{\infty} |y(hT_s) - y^*(hT_s)| \text{ such that: } M_S = 2 \qquad (21)$$

where $y(hT_s)$ is the system response and $y^*(hT_s)$ is the desired response, which is usually selected to fulfil a pre-defined control bandwidth. The main advantage of using the tuning procedures depicted in (20) and (21), is that identical loop robustness is achieved for both, the conventional and the proposed methodology.

In Fig. 7a the results obtained by implementing the conventional control strategy reported in [12], [19] are shown. In this case the mitigation currents are off-line calculated using (15) and the control systems are based on PI controllers implemented in the stationary frame. On the other hand, the results obtained by the mitigation currents regulated using the proposed control strategy are shown in Fig. 7b.

As shown in Fig. 7, the peak to peak value of each capacitor voltage is reduced in 55% from approximately 11.9V to 6.6V when the proposed mitigating method is applied. Notice that this reduction produces an increase of 11% in the cluster peak-to-peak currents (from 34.4A to 38.3A), because in this case the feed-forward currents of (15) were underestimated. Both stator machine currents depicted in Fig. 7 (22.3A peak-to-peak) shows little distortion and are well regulated.

As mentioned before, to test the performance of the proposed control systems some of the experimental results have been obtained considering a trapezoidal waveform in the common mode voltage. In this case the values of dv/dt are reduced and the cluster voltage does not have hard voltage transitions between levels. This is depicted in Fig. 8 (yellow signal), with the line-to-line voltage corresponding to the green signal. Notice that in Fig. 7 and Fig. 8 it is shown that
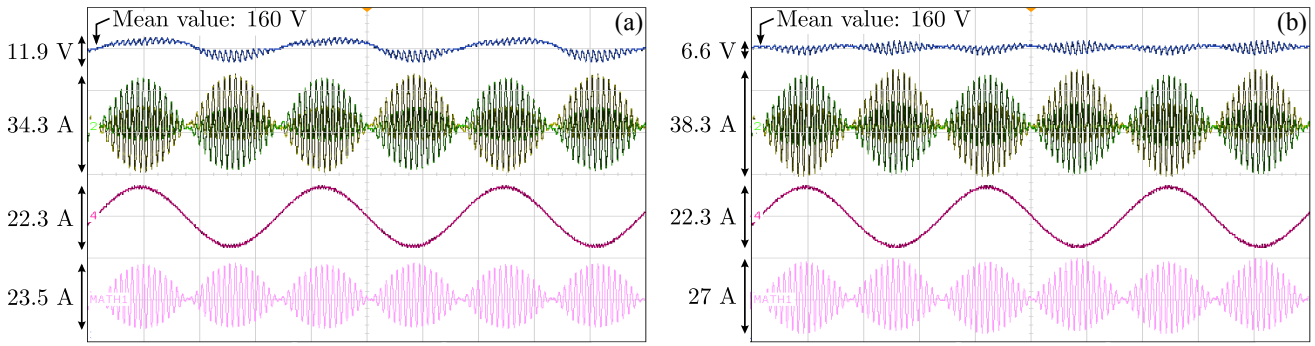
Fig. 7. M²C static performance at LFM. (a) stationary frame controllers (conventional methodology). (b) proposed control system. Blue: capacitor voltage (20 V/Div), yellow and green: cluster currents (15 A/Div), red: machine current (15 A/Div), pink: phase a circulating current (15 A/Div).
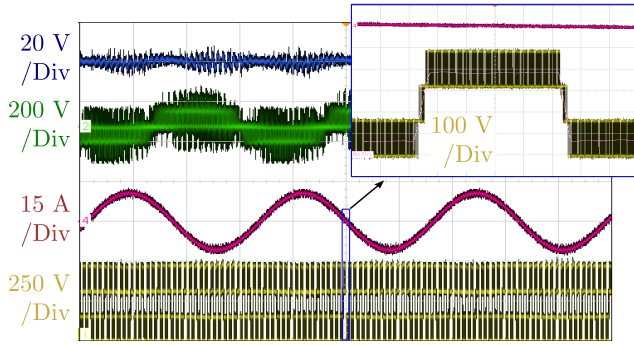

Fig. 8. M²C signals applying the proposed control system. Blue: capacitor voltage (20 V/Div). green: line to line voltage (200 V/Div), red: machine current (15 A/Div), yellow: cluster voltage (250 V/Div).
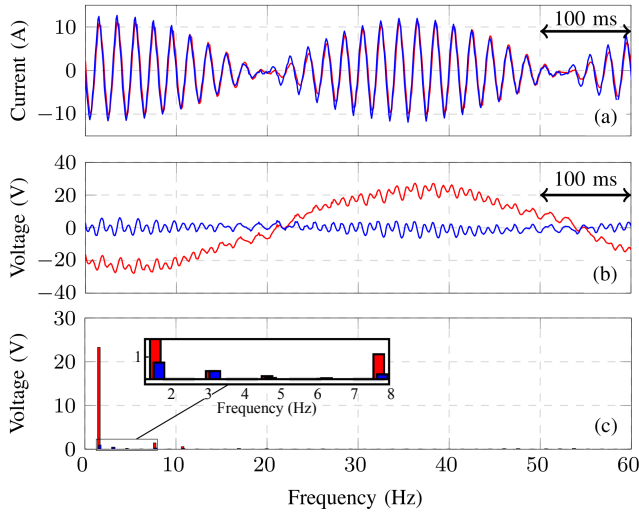

Fig. 9. Comparison of mitigation schemes. (a) i_α^Σ. (b) $v_{C\alpha}^\Delta$. (c) $v_{C\alpha}^\Delta$ Fourier Spectrum. Blue: dq-based control, red: stationary frame control.

the proposed control system is able to reduce the capacitor voltage oscillations even if the waveform of $\tilde{v}_0$ defined in (14) is modified. As explained before the dq-based voltage control loop regulates with zero steady state error the signals of frequency ω_e present in the voltage $\underline{v}_{C\alpha\beta}^\Delta$, even if variations in the M²C system are produced.

Finally an amplify view of some of the signals corresponding to the test of Fig. 7 are shown in Fig. 9. In Fig. 9a

both circulating currents are shown, i.e. that obtained from the conventional control method and the one obtained with the proposed control method of Fig. 2. The circulating currents have similar phase and different peak values. Fig. 9 (b) shows the voltage $v_{C\alpha}^\Delta$ achieved with both control methodologies. Notice that for the conventional control system, the 1.6Hz oscillations are not eliminate from the capacitor voltage. The Fourier analysis of the frequency components in $v_{C\alpha}^\Delta$, for both control methodologies, is shown in Fig. 9. For the conventional control methodology there is a 20V component at $f \approx 1.6$Hz, on the other hand the proposed control method has a 0.7V component at the same frequency.

B. Dynamic performance of the proposed control system

1) Performance considering step changes in the machine currents: The experimental results considering step changes in the machine currents are shown in Fig. 10. For this test is considered that initially all the capacitors are discharged and the control and start-up of the M²C is realised in four stages (t_0=0s, t_1=0.1s, t_2=0.6s, t_3=1.1s). In the first stage,$[t_0 \rightarrow t_1]$ (see at top of Fig. 10), the eighteen M²C cells (3 per cluster) are charged to 150V imposing a duty cycle of 50%, ($E = 450$V). During the second stage, $[t_1 \rightarrow t_2]$, the control loops to regulate the voltages $\underline{v}_{C\alpha\beta}^\Sigma$, $\underline{v}_{C\alpha\beta}^\Delta$, v_{C0}^Σ and v_{C0}^Δ are enabled and the cell voltage set-point is changed linearly from 150V to 160V (see Fig. 10(b)). In this stage a small sinusoidal component of 50Hz is superimposed in the dc input current to facilitate the regulation of v_{C0}^Δ. Moreover, as shown in Fig. 10(c) and Fig. 10(d), circulating current and common mode voltage are imposed in the system.

A step in the the reference of the machine magnetising current is realised in the third stage, $[t_2 \rightarrow t_3]$ and i_d^* is set to 2.2 A (see Fig. 10(e) and Fig. 10(f)). After this step change, the proposed mitigating algorithm increases the common mode voltage and the magnitude of the circulating currents to maintain the M²C capacitor voltages well regulated.

The last stage, $[t_3 \rightarrow t_4]$, is the machine start-up by imposing a constant torque current of 8.5A, as is shown in Fig. 10(e) and Fig. 10(f). In this stage the machine speed is increased to approximately 1600 rpm (see Fig. 10(a)). Notice that during LFM operation, which was defined below 10 Hz (close to 500 rpm), the magnitude of $\underline{i}_{\alpha\beta}^\Sigma$ is increased as the common mode voltage is reduced (see Fig. 10(c) and Fig. 10(d)).
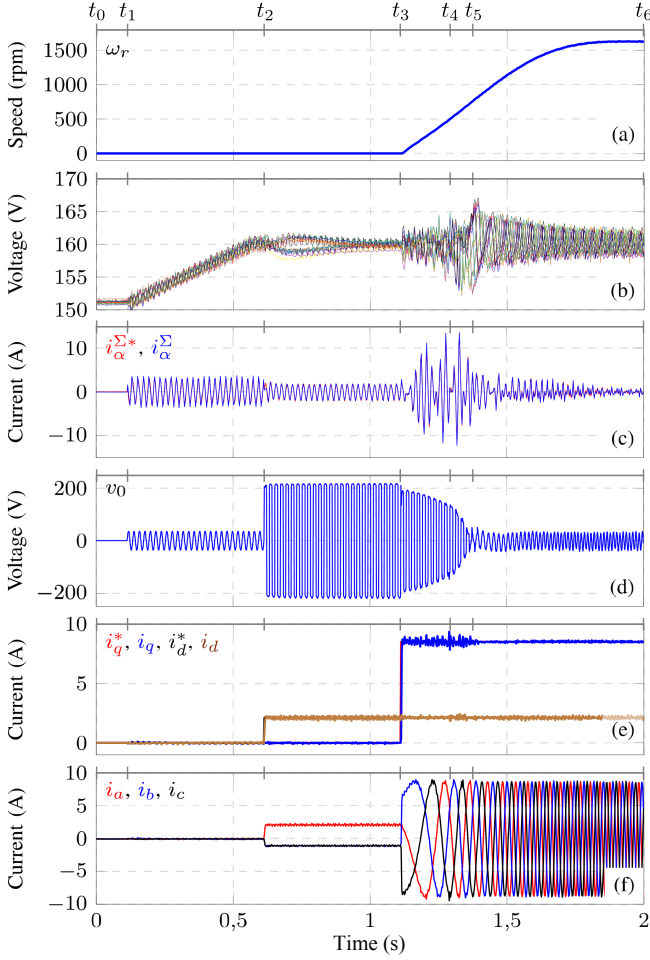
Fig. 10. Set-up response to step changes in the machine currents. (a) Machine speed, (b) capacitor voltages, (c) Circulating current i_α^Σ, (d) desired common mode voltage, (e) ac port current (dq-frame), (f) ac port current (abc-frame).

The transition mode (TM) is defined between 10Hz-15Hz. In this mode the amplitude of $\underline{i}_{\alpha\beta}^\Sigma$ is reduced and the magnitude of the capacitor voltage oscillations increases to approximately $\pm 4.44\%$ of the nominal value (160V). When HFM operation is achieved, the circulating currents required are of relatively small amplitude balancing the energy in the M²C cells. In addition, for HFM operation the current i^P is relatively large and, due to this, a low dc component in the common-mode voltage is enough to maintain the voltage v_{C0}^Δ well regulated (see (9d)).

2) Dynamic performance considering a ramp variation in ω_r^*: To test the performance of the M²C-based drive in the whole speed range, including zero-speed crossing operation, the rotational speed profile shown in Fig. 11(a) is applied to the induction machine. The machine is accelerated from 0 to ± 1700 rpm with a slope of ± 1800 rpm/s (see Fig. 11(a)). During LFM operation (below 10 Hz), a small ac component is superimposed in the dc input current to facilitate the regulation of v_{C0}^Δ (see Fig. 11(c) and Fig. 11(i)). Therefore some noise and oscillations are present in this current which are also related to the application of the common mode voltage. However, this is not a problem since the motor currents are not
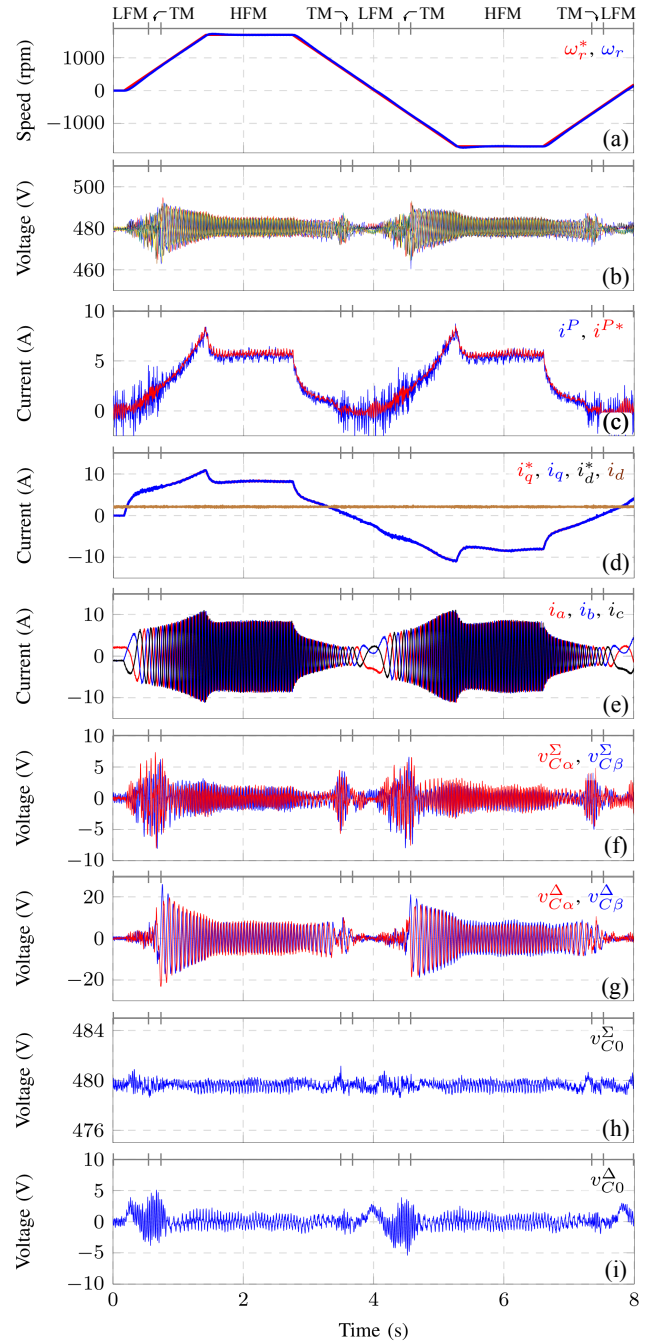

Fig. 11. System response to a ramp speed variation. (a) machine speed, (b) Total cluster voltages, (c) dc port current, (d) ac port current (dq frame), (e) ac port currents (abc frame), (f) $v_{C\alpha}^\Sigma$ and $v_{C\beta}^\Sigma$ voltages, (g) $v_{C\alpha}^\Delta$ and $v_{C\beta}^\Delta$ voltages, (h) v_{C0}^Σ voltage, (i) v_{C0}^Δ voltage.

affected (see Fig. 11(d) and Fig. 11(e)). Moreover, in this work is assumed that the dc port power supply can safely operate with (small) ac signals superimposed in i^P.

In Fig. 11(g) the $\alpha\beta$ components of the voltage vector $\underline{v}_{C\alpha\beta}^\Delta$ are depicted. These voltage components are well regulated during LFM operation, showing the effectiveness and good dynamic response of the proposed control system. Moreover, the voltages $\underline{v}_{C\alpha\beta}^\Sigma$ and v_{C0}^Σ are also tightly regulated (see Fig. 11(f) and Fig. 11(h)); hence, the total cluster voltages are well controlled for LFM operation, as shown in Fig. 11(b).

When the transition zone is reached, the output signals of the LFM/HFM control systems are weighted up by the factors k_l and k_h defined in (19). During this transition the oscillations of the cluster voltages are less than 30V peak-to-peak, representing a variation of $\pm 3.1\%$ respect to the nominal value ($3v_C^* = 480$V). During HFM operation, neither the ac component in i^P nor the mitigating signals of (15) are applied. Therefore, only the dc components of the $\Sigma\Delta\alpha\beta 0$ voltages are regulated. Moreover, the amplitude of the oscillations in the $\Sigma\Delta\alpha\beta 0$ voltages decreases when ω_r increases. Therefore they are relatively simpler to control. This is shown in Fig. 11(f) to Fig. 11(h) (depicting the voltages $v_{C\alpha\beta}^\Sigma$, $v_{C\alpha\beta}^\Delta$, v_{C0}^Σ and v_{C0}^Δ).

From the experimental results depicted in Fig. 11 is also concluded that the magnitudes of the oscillations produced when the machine is regenerating energy to the dc-link power source are smaller than those produce when the machine is motoring. This is because, for this test, the amplitudes of the machine currents and i^P current are reduced during regeneration.

To the best of our knowledge this is the first time that regenerative and zero-speed crossing operation of a M²C-based drive are experimentally implemented using a vector-controlled induction machine fed by a M²C.

V. CONCLUSION

In this paper a new and comprehensive vector-power-voltage (vPV) model of the M²C-based drive has been presented. Using this model is simple to analyse the converter dynamics and it can be used to design and implement vector control strategies to balance the power converter, mitigate low frequency voltage oscillations, regulate the input/output energy transfer, etc.

Using the vPV model, a novel dq-based vector control strategy for LFM operation has been presented, analysed and experimentally validated in this paper. This control methodology balances the capacitor voltages, as well as mitigates the low frequency (ω_e) capacitor voltage oscillations using nested control loops implementing PI and resonant controllers.

The proposed modelling and vector control systems have also been applied to HFM operation. In all the cases, i.e. LFM and HFM operation, decoupled control of the voltages in the $\Sigma\Delta\alpha\beta 0$-space is achieved by using circulating currents and common mode voltage of different frequencies. All the control strategies proposed in this paper have been analytically discussed and experimentally validated using a M²C-based drive prototype. The dynamic and steady state performance of the proposed control methodologies have been tested, considering M²C starting-up, step changes in both the torque and magnetising currents, speed-ramps, zero-speed crossing test, motoring and generating operation, rotor-locked operation, etc. In all the cases the performance achieved has been excellent.

When compared to the control strategies reported in the literature, the proposed control system produces a higher computational burden, which is mostly required to implement several controllers, and to transform current and voltage signals from abc coordinates to $\Sigma\Delta\alpha\beta 0$ and dq coordinates. However this extra computational burden can be easily handled by a modern DSP, e.g. in this work the implementation of the whole control system for an 18-cell converter, has been relatively simple to realise using a low cost commercial DSP augmented by FPGFA boards.

REFERENCES

[1] M. Glinka and R. Marquardt, "A new AC/AC-multilevel converter family applied to a single-phase converter,," in *Power Electronics and Drive Systems, 2003. PEDS 2003. The Fifth International Conference on*, vol. 1, DOI 10.1109/PEDS.2003.1282669, Nov. 2003, pp. 16–23.

[2] M. Glinka and R. Marquardt, "A new AC/AC multilevel converter family," *IEEE Trans. Ind. Electron.*, vol. 52, DOI 10.1109/TIE.2005.843973, no. 3, pp. 662–669, Jun. 2005.

[3] S. Debnath, J. Qin, and M. Saeedifard, "Control and Stability Analysis of Modular Multilevel Converter Under Low-Frequency Operation," *IEEE Trans. Ind. Electron.*, vol. 62, DOI 10.1109/TIE.2015.2414908, no. 9, pp. 5329–5339, Sep. 2015.

[4] M. Perez, S. Bernet, J. Rodriguez, S. Kouro, and R. Lizana, "Circuit Topologies, Modeling, Control Schemes, and Applications of Modular Multilevel Converters," *IEEE Trans. Power Electron.*, vol. 30, DOI 10.1109/TPEL.2014.2310127, no. 1, pp. 4–17, Jan. 2015.

[5] Y. Okazaki, W. Kawamura, M. Hagiwara, H. Akagi, T. Ishida, M. Tsukakoshi, and R. Nakamura, "Experimental Comparisons Between Modular Multilevel DSCC Inverters and TSBC Converters for Medium-Voltage Motor Drives," *IEEE Trans. Power Electron.*, vol. PP, DOI 10.1109/TPEL.2016.2562103, no. 99, pp. 1–1, 2016.

[6] K. Ilves, L. Bessegato, and S. Norrga, "Comparison of cascaded multilevel converter topologies for AC/AC conversion," in *Power Electronics Conference (IPEC-Hiroshima 2014 - ECCE-ASIA), 2014 International*, DOI 10.1109/IPEC.2014.6869722, May. 2014, pp. 1087–1094.

[7] B. Tai, C. Gao, X. Liu, and Z. Chen, "A Novel Flexible Capacitor Voltage Control Strategy for Variable-Speed Drives With Modular Multilevel Converters," *IEEE Trans. Power Electron.*, vol. 32, DOI 10.1109/TPEL.2016.2535463, no. 1, pp. 128–141, Jan. 2017.

[8] J. J. Jung, H. J. Lee, and S. K. Sul, "Control Strategy for Improved Dynamic Performance of Variable-Speed Drives With Modular Multilevel Converter," *IEEE Trans. Emerg. Sel. Topics Power Electron.*, vol. 3, DOI 10.1109/JESTPE.2014.2323955, no. 2, pp. 371–380, Jun. 2015.

[9] M. Hagiwara, K. Nishimura, and H. Akagi, "A Medium-Voltage Motor Drive With a Modular Multilevel PWM Inverter," *IEEE Trans. Power Electron.*, vol. 25, no. 7, pp. 1786–1799, Jul. 2010.

[10] H. Akagi, "New trends in medium-voltage power converters and motor drives," in *Industrial Electronics (ISIE), 2011 IEEE International Symposium on*, DOI 10.1109/ISIE.2011.5984128, Jun. 2011, pp. 5–14.

[11] N. Thitichaiworakorn, M. Hagiwara, and H. Akagi, "Experimental Verification of a Modular Multilevel Cascade Inverter Based on Double-Star Bridge Cells," *IEEE Trans. Ind. Appl.*, vol. 50, no. 1, pp. 509–519, January-February 2014.

[12] M. Hagiwara, I. Hasegawa, and H. Akagi, "Start-Up and Low-Speed Operation of an Electric Motor Driven by a Modular Multilevel Cascade Inverter," *IEEE Trans. Ind. Appl.*, vol. 49, no. 4, pp. 1556–1565, July-August 2013.

[13] A. J. Korn, M. Winkelnkemper, and P. Steimer, "Low Output Frequency Operation of the Modular Multi-Level Converter," in *Energy Conversion Congress and Exposition (ECCE), 2010 IEEE*. IEEE, Sep. 2010.

[14] A. Antonopoulos, L. Ängquist, S. Norrga, K. Ilves, L. Harnefors, and H.-P. Nee, "Modular Multilevel Converter AC Motor Drives With Constant Torque From Zero to Nominal Speed," *IEEE Trans. Ind. Appl.*, vol. 50, DOI 10.1109/TIA.2013.2286217, no. 3, pp. 1982–1993, May. 2014.

[15] B. Li, S. Zhou, D. Xu, D. Xu, and W. Wang, "Comparative study of the sinusoidal-wave and square-wave circulating current injection methods for low-frequency operation of the modular multilevel converters," in *2015 IEEE Energy Conversion Congress and Exposition (ECCE)*, DOI 10.1109/ECCE.2015.7310324, Sep. 2015, pp. 4700–4705.

[16] S. Debnath, J. Qin, and M. Saeedifard, "Control and Stability Analysis of Modular Multilevel Converter Under Low-Frequency Operation," *IEEE Trans. Ind. Electron.*, vol. 62, DOI 10.1109/TIE.2015.2414908, no. 9, pp. 5329–5339, Sep. 2015.

[17] A. Antonopoulos, L. Ängquist, L. Harnefors, and H. P. Nee, "Optimal Selection of the Average Capacitor Voltage for Variable-Speed Drives With Modular Multilevel Converters," *IEEE Trans. Power Electron.*, vol. 30, DOI 10.1109/TPEL.2014.2316273, no. 1, pp. 227–234, Jan. 2015.

[18] J. Kolb, F. Kammerer, and M. Braun, "Dimensioning and design of a Modular Multilevel Converter for drive applications," in *Power Electronics and Motion Control Conference (EPE/PEMC), 2012 15th International*, DOI 10.1109/EPEPEMC.2012.6397380, Sep. 2012, pp. 1–8.

[19] J. Kolb, F. Kammerer, M. Gommeringer, and M. Braun, "Cascaded Control System of the Modular Multilevel Converter for Feeding Variable-Speed Drives," *IEEE Trans. Power Electron.*, vol. 30, DOI 10.1109/TPEL.2014.2299894, no. 1, pp. 349–357, Jan. 2015.

[20] S. Du, B. Wu, K. Tian, N. R. Zargari, and Z. Cheng, "An Active Cross-Connected Modular Multilevel Converter (AC-MMC) for a Medium-Voltage Motor Drive," *IEEE Trans. Ind. Electron.*, vol. 63, DOI 10.1109/TIE.2016.2547875, no. 8, pp. 4707–4717, Aug. 2016.

[21] R. Cardenas, C. Juri, R. Pena, J. Clare, and P. Wheeler, "Analysis and Experimental Validation of Control Systems for Four-Leg Matrix Converter Applications," *IEEE Trans. Ind. Electron.*, vol. 59, DOI 10.1109/TIE.2011.2158041, no. 1, pp. 141–153, Jan. 2012.

[22] M. Espinoza, A. Mora, M. Diaz, and R. Cárdenas, "Balancing energy and low frequency operation of the Modular Multilevel Converter in Back to Back configuration," in *Ecological Vehicles and Renewable Energies (EVER), 2015 International Conference on*, DOI 10.1109/EVER.2015.7113005, Mar. 2015, pp. 1–9.

[23] F. Kammerer, M. Gommeringer, J. Kolb, and M. Braun, "Energy balancing of the Modular Multilevel Matrix Converter based on a new transformed arm power analysis," in *Power Electronics and Applications (EPE'14-ECCE Europe), 2014 16th European Conference on*, DOI 10.1109/EPE.2014.6910939, Aug. 2014, pp. 1–10.

[24] Y. Wan, S. Liu, and J. Jiang, "Generalised analytical methods and current-energy control design for modular multilevel cascade converter," *IET Power Electronics*, vol. 6, DOI 10.1049/iet-pel.2012.0494, no. 3, pp. 495–504, Mar. 2013.

[25] H. Akagi, S. Inoue, and T. Yoshii, "Control and Performance of a Transformerless Cascade PWM STATCOM With Star Configuration," *IEEE Trans. Ind. Appl.*, vol. 43, DOI 10.1109/TIA.2007.900487, no. 4, pp. 1041–1049, Jul. 2007.

[26] Y. Okazaki, H. Matsui, M. M. Muhoro, M. Hagiwara, and H. Akagi, "Enhancement on capacitor-voltage-balancing capability of a modular multilevel cascade inverter for medium-voltage synchronous-motor drives," in *2015 IEEE Energy Conversion Congress and Exposition (ECCE)*, DOI 10.1109/ECCE.2015.7310550, Sep. 2015, pp. 6352–6359.

[27] R. Cardenas, R. Pena, J. Clare, and P. Wheeler, "Analytical and Experimental Evaluation of a WECS Based on a Cage Induction Generator Fed by a Matrix Converter," *IEEE Trans. Energy Convers.*, vol. 26, DOI 10.1109/TEC.2010.2083666, no. 1, pp. 204–215, Mar. 2011.

[28] A. G. Yepes, F. D. Freijedo, Ó. Lopez, and J. Doval-Gandoy, "Analysis and Design of Resonant Current Controllers for Voltage-Source Converters by Means of Nyquist Diagrams and Sensitivity Function," *IEEE Trans. Ind. Electron.*, vol. 58, DOI 10.1109/TIE.2011.2126535, no. 11, pp. 5231–5250, Nov. 2011.

[29] B. Kristiansson and B. Lennartson, "Robust and optimal tuning of PI and PID controllers," *IEE Proceedings - Control Theory and Applications*, vol. 149, DOI 10.1049/ip-cta:20020088, no. 1, pp. 17–25, Jan. 2002.

Roberto Cárdenas (S'95-M'97-SM'07) was born in Punta Arenas Chile. He received his B.Sc. degree from the University of Magallanes, Chile, in 1988 and his Msc. and Ph.D degrees from the University of Nottingham in 1992 and 1996 respectively. From 1989-1991 and 1996-2008 he was a lecturer in the University of Magallanes Chile. From 1991 to 1996 he was with the Power Electronics Machines and Control Group (PEMC group), University of Nottingham, United Kingdom. From 2009-2011 he was with the Electrical Engineering Department, University of Santiago. He is currently a professor of power electronics and drives in the Electrical Engineering Department, University of Chile, Chile. His main interests are in control of electrical machines, variable speed drives and renewable energy systems.

Matías Díaz (S'15) was born in Santiago, Chile. He received the B.Sc. and the M.Sc. degrees from the University of Santiago of Chile in 2011. Currently, he is pursuing a dual Ph.D. degree at the University of Nottingham, U.K., and at the University of Chile, Chile. From 2013 to 2015 he was sub-director of the School of Engineering at Duoc UC. Currently, he is a Lecturer at the University of Santiago of Chile. His main research interests include the control of Wind Energy Conversion Systems, Multilevel Converters, and renewable energy systems.

Jon C. Clare (M'90-SM'04) was born in Bristol, U.K., in 1957. He received the B.Sc. and Ph.D. degrees in electrical engineering from the University of Bristol, Bristol. From 1984 to 1990, he was a Research Assistant and Lecturer with the University of Bristol, where he was involved in teaching and research on power electronic systems. Since 1990, he has been with the Power Electronics, Machines and Control Group, The University of Nottingham, Nottingham, U.K., where he is currently a Professor of power electronics. His research interests include power-electronic converters and modulation strategies, variable-speed-drive systems, and electromagnetic compatibility.

Mauricio Espinoza (S'15) was born in Alajuela, Costa Rica. He received the B.Sc. and Lic. degrees in electrical engineering from the University of Costa Rica in 2010 and 2012 respectively. From 2010-2014 he was a lecturer in the University of Costa Rica. Actually, he is pursuing a Ph.D. degree at the University of Chile, Chile. During his career, he has worked in research projects related to Modular Multilevel Converters, machine modelling and control systems for power electronics.